Polymorphic self-organization of a lauroyl peptide in response to pH and concentration.

Federica Novelli[†,¥], Alessandro Strofaldi[†,◇], Serena De Santis[†,§], Alessandra Del Giudice[†], Stefano Casciardi[‡], Luciano Galantini[†], Stefano Morosetti[†], Nicolae V. Pavel[†], Giancarlo Masci[†,], Anita Scipioni[†,]**

† Dipartimento di Chimica, Sapienza Università di Roma, P.le A. Moro, 5, Rome, Italy

‡ National Institute for Insurance against Accidents at Work (INAIL Research), Department of Occupational and Environmental Medicine, Epidemiology and Hygiene, Rome, Italy

KEYWORDS. lipopeptide, peptide amphiphile, β-sheet conformation, pH-sensitive peptide conformation, core-shell morphology, pH-sensitive morphology, sol-gel transition, hydrogel.

ABSTRACT. Amphipathic peptides are attractive building blocks for the preparation of self-assembling, bio-inspired and stimuli responsive nano-materials with pharmaceutical interest. The bioavailability of these materials can be improved with the insertion of D amino acid residues to avoid fast proteolysis in vivo. With this knowledge, a new lauroyl peptide consisting of a sequence of glycine, glycine, D-serine, and D-lysine was designed. In spite of its simple sequence, this lipopeptide self-assembles into spherical micelles at acid pH, when the peptide moiety adopts disordered conformations. The self-aggregates reshape towards fibers at basic pH following the conformational transition of the peptide region from random coil to β-sheet. Finally, hydrogels are achieved at basic pH and higher concentrations. The transition from random coil to β-sheet conformation of the peptide headgroup obtained by increasing pH was monitored by circular dichroism and vibrational spectroscopy. A structural analysis, performed

by combining dynamic light scattering, small angle X-ray scattering, transmission electron microscopy and molecular dynamic simulations, demonstrated that the transition allows the self-assemblies to remodel from spherical micelles to rod-like shapes, to long fibers with rectangular cross section and a head-tail-tail-head structure. The viscoelastic behavior of the hydrogels formed at the highest pH was investigated by rheology measurements.

INTRODUCTION

Among the wide world of amphiphilic building blocks that self-assemble according to a bottom-up process, amphipathic peptides attract interests to achieve bio-inspired nano-materials with potential pharmaceutical applications.[1-5] However, their use is hindered from their reduced bioavailability owing to a fast clearance in vivo. Different strategies are explored to enhance the metabolic stability of peptide-based nano-systems such as the insertion of D amino acid residues[6] or β-peptoids.[7] The conjugation with lipids is an alternative approach.[7-10] Lipidation provides hybrids with amphiphilic character that ensures their self-assembly in stable nano-aggregates with core-shell morphology.[11,12] Owing to their bioactivity, biospecificity and reduced toxicity, nano-structures obtained by self-assembling of natural and synthetic lipopeptides have important therapeutic applications including drug and gene delivery, diagnostics, tissue engineering and regenerative medicine[11-15] and cosmetics.[16-20] Applications in pharmaceutics are also shown by synthetic and bacterial-expressed lipopeptides with antimicrobial, antibiotic and antifungal activity.[21,22]

The lipopeptides are peptide-based molecules where the peptide moiety forms the hydrophilic headgroup. A proper design of amino acid sequence allows obtaining well-ordered self-assemblies with morphology and properties that can be tuned by changing pH, temperature,

concentration, and ionic strength.[12,23-31] The hydrocarbon chains, covalently linked either to the peptide backbone or to the side chains, triggers the self-aggregation in aqueous solutions and induces and stabilizes secondary and tertiary structures also in short peptide sequences.[32] The alkyl tail length affects structures and functions of the self-aggregates since morphology and surface features depend on the fine balance of dipole-dipole, electrostatic, π-π stacking, hydrophobic and hydrogen bond interactions.[23,24,26,33,34] Steroidal moieties can be also used as hydrophobic block to provide molecules with a self-assembly behavior merging the complex aggregation features of steroidal surfactants and peptides.[35,36]

The hydrophobic interactions among the aliphatic chains are important to promote the self-assembly of lipopeptides.[12] However, the role of the secondary structures of the peptide component[37,38] and the hydrogen bonds[39] was also shown to be crucial. Accordingly, different morphology and mechanical properties of nano-structures are obtained when headgroup secondary structures re-organize following changes of peptide sequences, pH and ionic strength. Evolution with time is also possible as recently shown for self-assemblies obtained by a gemini-type lipopeptide.[40]

Charged amino acid residues and peptide sequences with propensity to assume pH-dependent *β*-sheet conformation are common motives in amphiphilic lipopeptides[23,37,38] for which spherical and worm-like micelles, vesicles, planar bilayers, nano-fibers and nano-tapes are observed to form. As regards elongated assemblies, their structural features mainly depend on the hydrocarbon chain length, the propensity of the peptide sequence to assume a *β*-sheet conformation and the electrostatic interactions among the polar heads. Often, gels arise by the self-assembly of high-aspect ratio structures, which provide topological interactions, forming a fiber network.[23,41]

This work reports the synthesis and structural characterization of the peptide amphiphile (PA) lauroyl-Gly-Gly-D-Ser-D-Lys-NH_2 TFA salt (C_{12}-GG**SK**, where the D residues are in bold, Figure 1). The lipopeptide was conceived for applications in nano-medicine. It was designed to self-organize in aqueous solutions into structures that reshape upon changes of pH, concentration and temperature. The aliphatic tail was conjugated to the N-terminus to induce the hydrophobic collapse and favor the self-assembly in core-shell morphologies. D amino acid residues were inserted to increase the resistance of the peptide region to proteolysis.[6] Furthermore, the different nano-structures could find applications in drug delivery by exploiting the presence of a hydrophobic core to encapsulate apolar drugs.[23,30] The peptide sequence of the headgroup was designed to obtain a pH-dependent random coil-β-like conformational transition ruled by the different degree of ionization of the ε-amino group of the lysine residue while the serine was introduced for their robust gelation property.[42] Both residues improve the solubility of the conjugate in water.

C_{12}-GG**SK** self-assemblies change morphologies in response to pH and concentration although its molecular structure is simple. Spherical micelle self-assemblies, obtained at acid pH, rearranged into fibers and, finally, into gel, when pH and concentration were increased. This is an interesting behavior since peptide amphiphiles with headgroups that have a strong tendency to adopt β-sheet conformations prevalently self-organize into elongated structures.[37] Furthermore, it is worthy of consideration that the position of the single amino acid residues and the site of the conjugation are relevant in the self-assembly behavior of stimuli-responsive lipopeptides, as recently reviewed.[12]

The physicochemical properties and conformations of the peptide headgroups were assessed. The critical aggregation concentration (cac) of C_{12}-GG**SK** was determined by fluorescence

spectroscopy whilst the secondary structure of the peptide moiety was investigated by circular dichroism and vibrational spectroscopy. Structure, size, and morphology of the self-aggregates were assessed by small angle X-ray scattering, dynamic light scattering, and transmission electron microscopy at different pHs and concentrations of the lipopeptide. Molecular dynamics simulations were carried out on uncharged lipopeptide to investigate the self-assembly at basic pH. Finally, the rheological properties of hydrogels formed at basic pH and their thermal sensitivity were investigated.

EXPERIMENTAL SECTION

Materials. Peptide synthesis grade *N*,*N*-dimethylformamide (DMF), trifluoroacetic acid (TFA), dichloromethane (DCM), 1-methyl-2-pyrrolidone (NMP), diethyl ether, *N*,*N*,*N'*,*N'*-tetramethyl-O-(benzotriazol-1-yl)uronium tetrafluoroborate (TBTU), *N*,*N*-diisopropylethylamine (DIPEA), triethylamine (TEA), 4-(dimethylamino)pyridine (DMAP), triisopropylsilane (TIS) were purchased from Aldrich and used as provided. Spectrograde pyrene and piperidine were from Fluka and distilled before use. DCM and DMF were dried with 4 Å molecular sieves. Rink-amide resin (1% DVB, 200-400 mesh and loading level 1.1 mmol·g^{-1}) and Amberlite IRA-67 ion-exchange resin were purchased from Aldrich. Fmoc-D-Ser-OH, Fmoc-D-Lys-OH and Fmoc-Gly-OH amino acids were from Bachem. Lauric acid was from Merck. Deuterated solvents for NMR spectroscopy were from Aldrich. Acetonitrile (MeCN, Chromasolv Plus, for HPLC) and spectrograde methanol (MeOH) were purchased from Aldrich and used as provided. Thin Layer Chromatography (TLC) was performed on silica gel Merck 60 F254 plates.

Synthesis of lauroyl-Gly-Gly-D-Ser-D-Lys(TFA)-NH_2. The lipopeptide C_{12}-GG**SK** was synthetized manually at 0.5 mmol scale on Rink amide polystyrene resin employing a standard

Fmoc methodology according to the scheme described in Figure S1. Before the synthesis, the resin was swollen in NMP for 30 min and then washed with DMF (three times) and DCM (three times). The coupling of the first amino acid was carried out using 3 equiv (relative to the resin loading) of Fmoc-D-Lys(Boc)-OH amino acid, 3 equiv of TBTU and 3.5 equiv of DIPEA in NMP for 3 h. All subsequent couplings were performed using 3 equiv of the appropriate Fmoc protected amino acids, 3 equiv of TBTU and 3.5 equiv of DIPEA in NMP under mechanical shaking for 3 h at room temperature and repeated twice. Fmoc deprotection was obtained by piperidine in DMF ((20% v/v, 5 mL, 2 times, 15 min) and the completion of the coupling reactions was checked by the ninhydrin-Kaiser test. After the peptide portion was completed, the N-terminus was capped with lauryl acid using the same reaction conditions described above. Cleavage and deprotection of the expected lipopeptide as TFA salt from the resin were achieved using a mixture of TFA, MilliQ water, and TIS in the ratio of 95/2.5/2.5 (5 mL, 3 h). The solution was collected by filtration, concentrated in vacuum to a viscous solution, and the lipopeptide was precipitated with cold diethyl ether. After repeated washing with diethyl ether, the precipitate was dissolved in water/dioxane 1/1 (v/v) and freeze-dried. The lipopeptide was identified by monodimensional ^{1}H NMR spectroscopy (Figure S2) and electrospray ionization mass spectrometry (Figure S3).

Preparation of the solutions. C_{12}-GG**SK** was dissolved in Milli-Q water to the desired concentration. The pH of each solution was corrected by addition of 0.1 M HCl or 0.01 and 0.1M NaOH and measured by CRISON pH meter after stabilization. The solutions used to measure the rheological properties were brought to basic pH and sonicated for 5 minutes to avoid the formation of precipitates before rheological measurements.

Fourier Transform-Infra Red Spectroscopy (FT-IR). Vibrational spectra were obtained with a Shimadzu FT-IR 8400S spectrometer equipped with attenuated total reflectance (ATR) Golden Gate in the 4000-650 cm^{-1} spectral range collecting eight interferograms with a 2 cm^{-1} resolution. Spectra were elaborated with Shimadzu IR Solution 1.1 software. ATR FT-IR spectra were recorded on dried films achieved by deposition of C_{12}-GG**SK** solutions in D_2O at different pHs.

Circular Dichroism (CD) Spectroscopy. CD spectroscopy was employed to investigate the transition from random coil-β-like conformation of C_{12}-GG**SK** and thermal stability of the gel formed at basic pH. The C_{12}-GG**SK** solutions were added with 0.01 $mol \cdot L^{-1}$ NaOH solution and left 2 minutes before recording the CD spectrum. The CD spectra were run with a JASCO J 715 spectropolarimeter equipped with a Peltier device for temperature control using quartz cells of 0.001, 0.01, 0.02, 0.1, 0.2 cm. Measurements were run in the 250-190 nm spectral range at constant temperature and an instrument scanning speed of 100 nm/min, with a response time of 1 s and bandwidth of 1 nm. Temperature scans were obtained with a speed of 1 $°C \cdot min^{-1}$. Spectra were reported in molar ellipticity.

Fluorescence Spectroscopy. Steady-state fluorescence spectra were measured on a Cary Eclipse (Varian) spectrofluorimeter equipped with a thermostated cell compartment and a SUPRASIL® quartz cell (10 × 4 mm). The fluorescence spectroscopy was used to evaluate the cac of C_{12}-GG**SK** (TFA salt) using pyrene as a probe according to a well-established method for core-shell nano-particles.[43] The fluorescence emission spectra of pyrene were measured in the spectral region 350-450 nm using λ_{exc}=335 nm. The lipopeptide was dissolved in an aqueous solution of $5 \cdot 10^{-7}$ $mol \cdot L^{-1}$ of pyrene in the concentration range $2 \cdot 10^{-6}$ - $4 \cdot 10^{-3}$ $mol \cdot L^{-1}$ and left under stirring overnight to obtain a constant value of the emission intensity.

Nuclear Magnetic Resonance (NMR) Spectroscopy. One-dimensional ^{1}H spectra were obtained on a VARIAN MERCURY spectrometer operating at 300.13 MHz. Chemical shifts were reported in parts per million (ppm) with respect to the residual undeuterated solvent used as an internal standard. Samples were prepared by dissolving about 5 mg of the lipopeptide in 0.5 mL of d_6-DMSO.

ESI-Mass Spectrometry (ESI-MS). ESI-MS spectra were performed on a Q-Tof Micro spectrometer (Micromass, now Waters) equipped with an electron spray ionization (ESI) source, in the positive ion mode. Data were analyzed using the MassLynx software (Waters). Mass spectra were run in the range of *m/z* 200-1400.

Dynamic Light Scattering (DLS). DLS experiments were carried out with a Brookhaven Instruments Corp. BI-200SM goniometer equipped with a BI-9000AT digital correlator. A 125 mW, 532 nm solid-state laser was used. Scattering angle θ was 90°. Cumulants analysis or CONTIN were used to fit the data. DLS measurements were carried out on aqueous solutions of C_{12}-GG**SK** at a concentration of 10 $mg \cdot mL^{-1}$. The pH was adjusted at 3 with 0.1 $mol \cdot L^{-1}$ HCl. The lipopeptide solutions were sonicated (UTA 18 sonicator, 280 W, FALC INSTRUMENTS) for 5 minutes and filtered with 0.45, 0.1 and 0.03 μm filters (Durapore, Millipore, USA) before measurements. All the measurements were carried out at 25±0.1 °C.

Energy Filtered-Transmission Electron Microscopy (EF-TEM). TEM micrographs were obtained with a Tecnai 12 G2 Twin Transmission Electron Microscope, operating at 120 keV. A droplet of a solution of C_{12}-GG**SK** in water was deposited onto a 400 mesh carbon coated copper grid. The excess of liquid was removed by placing the grid onto a filter paper and left to dry in air at room temperature for a few minutes. Samples were negatively stained with 2% w/v phosphotungstic acid (PTA) buffered at pH 7.3.

Lipopeptide solutions were imaged at the concentrations of $7 \cdot 10^{-4}$ mol·L^{-1} and $1.6 \cdot 10^{-3}$ mol·L^{-1} at pH 3 and 8.4. pH was adjusted with 0.1 mol·L^{-1} HCl and NaOH solutions.

Scanning Electron Microscopy (SEM). SEM micrographs were recorded with a ZEISS AURIGA 405 microscope (0.5-30 keV, 10^{-10} mbar). The solution of C_{12}-GG**SK** in Milli-Q water at a concentration of $3.1 \cdot 10^{-3}$ mol·L^{-1} was brought to pH 11 and left at room temperature to allow the gel formation. Then, the gel was quickly frozen in liquid nitrogen, broken with cold tweezers and fragments of the frozen gel were freeze-dried in high vacuum. Afterwards, the dried samples were mounted on aluminum SEM stubs using conductive carbon tape and imaged.

Rheological measurements. Rheological experiments performed with a Bohlin CS10 stress controlled rheometer using a concentric cylinder measuring system (C14). Temperature was controlled within ± 0.1 °C. The solution in the measuring geometry was isolated by a Teflon septum to prevent solvent evaporation. About 3 ml of samples were charged. Storage and loss moduli, G' and G", were determined as a function of time at a fixed frequency 0.01 or 1 Hz. Frequency sweep measurements were done in the range 0.1 - 10 Hz. Both experiments were performed at fixed stress, starting from the lower value 0.2 Pa in the first stage of gelation and progressively increasing it up to 1 Pa as gelation proceeds. Strain was kept below 1 % after gel point was reached to avoid slipping or gel fractures.

Rheological measurements were carried out on 2 mg·mL^{-1} ($3.2 \cdot 10^{-3}$ mol·L^{-1}) lipopeptide solutions after filtration on 0.45 μm filters (Durapore Millipore). Gel points were measured after bringing the pH to 11.0 with a 0.1 mol·L^{-1} NaOH solution.

Stress-sweep experiments on completely formed gels were done in order to be sure to perform measurements in the range of linear viscoelasticity. The absence of any slipping was determined

by creep tests. Frequency sweep and temperature sweep experiments were carried out on a lipopeptide solution brought to pH 11 and left overnight before the measurement.

Small Angle X-ray Scattering (SAXS). SAXS measurements were performed on 25 $mg \cdot mL^{-1}$ ($3.9 \cdot 10^{-2}$ $mol \cdot L^{-1}$) C_{12}-GG**SK** water solution at spontaneous pH after filtration on 0.45 μm filters (Durapore Millipore) and on the gel sample obtained by bringing the $6.0 \cdot 10^{-3}$ $mol \cdot L^{-1}$ solution of C_{12}-GG**SK** to pH 11.

The data were collected at the SWING beamline of Synchrotron SOLEIL (Gif-sur-Yvette, France), with an X-ray wavelength λ=1.033 Å. Data were collected in the scattering vector range $0.023 < q < 3.9$ nm^{-1}, where $q = 4\pi\sin(\theta)/\lambda$ and 2θ is the scattering angle. A second configuration with detector distance set to 55 cm allowed for improvement of the data quality in the q range 0.2-0.4 $Å^{-1}$ for the gel sample. In the first case (C_{12}-GG**SK** water solution at spontaneous pH) the measurements were performed using the automated sample loader provided at the beamline and the images were captured with 500 ms exposures by the AVIEX170170 CCD. In the second case (C_{12}-GG**SK** gel at pH 11), the measurements were performed by loading the sample in disposable quartz capillaries with 2.0 mm diameter; scattering frames were collected with 10 exposures of 490 ms on an Eiger 4M detector (Dectris). In both cases Milli-Q water was used to collect the background data for subtraction. The SAXS data reduction (radial integration, absolute scaling, frames selection and averaging, background subtraction) was performed using the FoxTrot software developed at the SOLEIL synchrotron.

The Indirect Fourier Transform (IFT) method implemented in the ITP program[44] was used for interpreting the SAXS curves. With this method, the pair-distance distribution function of the single scattering particle $p(r)$ is extracted by indirect Fourier transform of the scattered intensity

$I(q)$ profile. The $p(r)$ adopts the value of zero at distances greater than the maximum size of the particle D_{max} and permits the determination of its electronic gyration radius R_g as

$$R_g = \left[\frac{\int_0^\infty r^2 p(r)dr}{2\int_0^\infty p(r)dr}\right]^{1/2}$$

The SAXS curves were also interpreted by assuming model form factors for the scattering aggregates and performing an optimization of the model parameters to fit the experimental data by means of the software SasView 4.1.0. [SasView, *http://www.sasview.org/*]. Negligible effects of interparticle interactions were considered in the fit, thus assuming $I(q) = kP(q)$ where $P(q)$ is the particle form factor and k is a constant accounting for particle concentration. For core-shell spherical particles the form factor depends on the geometrical parameters core radius and shell thickness, and on the scattering length density of core and shell. The form factor expressions for this particle geometry has been carefully described and extensively used to interpret the SAXS curves of self-assembling systems.[45]

A core-shell parallelepiped form factor was also used as a model for elongated ribbon nano-structures. In addition, the inspection of the Guinier plots valid for rod-like and lamellar objects helped discerning the most suitable morphology and, in case of an acceptable linear fit, provided estimates of the radius of gyration of the cylindrical (R_c) or lamellar (R_t) cross-sections. These fits were performed with the software PRIMUS.[46]

Molecular Dynamics (MD) Simulations. All-atom MD simulations were performed for C_{12}-GG**SK** in water by using GROMACS 4.5.6 software package adopting the force field GROMOS96 54a7.[47] The lauroyl chain was modeled using the force field proposed for the simulation of dipalmitoylphosphatidylcholine (DPPC) bilayers[48,49] that was used in conjunction with GROMOS96 54a7.

D-Ser and D-Lys residues were generated imposing the correct value of the improper dihedral angles and the corresponding parameters were introduced in residuestype.dat, aminoacids.rtp, aminoacids.hdb files of GROMOS package.

A cylindrical micelle formed of 72 parallel lipopeptide molecules was adopted as the initial condition for the MD simulations and considered as the representative section of a rod-like structure (Figure S4). To this end, the size of z-axis (perpendicular to the top surface of the micelle) was adjusted to have van der Waals distances between each adjacent cell whilst the *x*- and *y*-axis, lying on the rod section, were large enough to avoid lateral adhesion of the aggregates. The β-sheet conformation was imposed to the peptide headgroup.

After thermalization and 150 ps equilibration steps on a *NVT* ensemble and subsequent 150 ps equilibration steps on *NPT* ensemble, a 50 ns MD simulation was performed at neutral pH in a periodic box of 9.7 × 9.7 × 3.3 nm size with 8220 water molecules, 1 Na^+ and 1 Cl^- to simulate the ionic strength. Periodic boundary conditions at constant volume and temperature (T=300 K) were imposed to the system and the Particle Mesh Ewald algorithm was employed in dealing with the long-range Coulomb interactions.[50] The integration time step was 2 fs.

All the aggregate structures were provided using the PyMol Molecular Graphics System.[51]

RESULTS AND DISCUSSION

The molecular structure of the lipopeptide C_{12}-GG**SK** is shown in Figure 1. C_{12}-GG**SK** was synthesized as sketched in Figure S1 and identified by monodimensional ^1H NMR spectroscopy (Figure S2) and electrospray ionization mass spectrometry (Figure S3). The self-assembling properties of the lipopeptide were tuned by inserting the pH sensitive lysine residue in the headgroup. A pH-dependent random coil-β-like conformational transition was ruled by the

different degree of ionization of the ε-amino group of the lysine residue. As a matter of fact, morphological transitions occur upon changes of pH and lipopeptide concentration. Furthermore, the presence of serine promotes the sol-gel transition and stabilizes the hydrogel.[42]

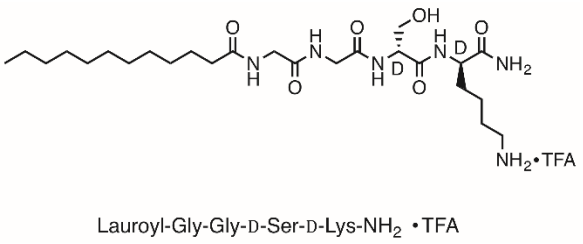

Figure 1. Chemical structure of the lipopeptide C_{12}-GG**SK**.

CD measurements. CD spectroscopy was used to investigate the conformation of the lipopeptide C_{12}-GG**SK** at different pHs and concentrations. Far UV CD spectra of C_{12}-GG**SK** in water recorded at a concentration greater than the cac and different pHs were overlaid in Figure 2A. At acid pH, the CD spectrum of the positively charged lipopeptide showed the typical strong positive band at about 200 nm associated to a prevalent random coil conformation for peptide sequence with D amino acid residues (pH=5.8, bold red line of Figure 2A)). When pH increased by addition of concentrated NaOH solution, a gradual variation of the spectra occurred leading to an inversion of the band at about 200 nm and the appearance of a positive band around 220-215 nm (pH=11.0, dashed blue line of Figure 2A). The final spectrum was assignable to a β-like conformation. Importantly, the presence of an isodichroic point observed at about 210 nm indicated the occurrence of a two-state thermodynamic equilibrium between random coil and β-like conformation. A sigmoidal trend was obtained reporting the molar ellipticity measured at

218 nm versus pH (Figure 2B). This result suggested that the conformational transition of the peptide headgroup was cooperative. The apparent inflection point, indicating a 50 % conversion from random coil to β-like conformation, was at pH 8.1 as obtained by the fitting curve.

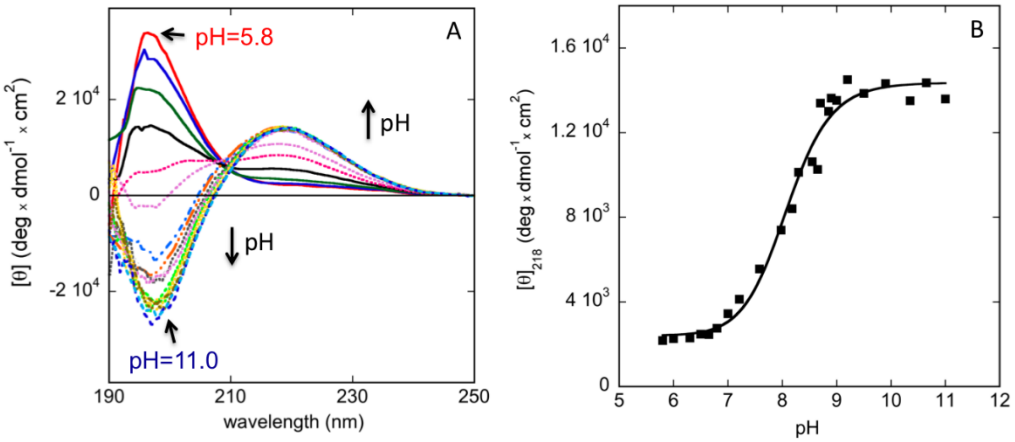

Figure 2. (A) Far UV CD spectra of C_{12}-GG**SK** water solution at different pH, the initial and final pH values are reported in the insert; (B) trend of the molar ellipticity measured at the wavelength of 218 nm as a function of pH and corresponding fit with a sigmoidal function. The initial concentration of the lipopeptide was $7.8 \cdot 10^{-4}$ mol·L^{-1}; the small effects of the dilution due to the addition of NaOH solution were considered to calculate the molar ellipticity. The spectra were run at T=20 °C.

As a result of the uncharged lysine residue at pH 11 and reduced electrostatic repulsions, the solution became more viscous and a sol-gel transition occurred slowly within 12 h at the spectroscopic concentration ($7.8 \cdot 10^{-4}$ mol·L^{-1}). The formation of hydrogel indicated that the transition towards the *β*-like conformation, when the lysine residue is uncharged, induced the self-assembly in high-aspect ratio structures, as will be confirmed by TEM micrographs and SAXS results, through a network of inter-peptide hydrogen bonds. The CD spectra recorded

soon at the end of the titration at 15 °C (black dashed line) and after 12 h to allow the gel to form (black bold line) at the same temperature were similar as illustrated in Figure S5A.

A temperature scan from 15 up to 80 °C was also carried out to evaluate the thermal stability of the gel. The molar ellipticity measured at 218 nm as a function of the temperature provided a sigmoidal trend with an inflection point at ≈50 °C (Figure S5B) suggesting that a thermally induced pseudo first-order transition towards unordered conformation occurred along with a gel-sol transition. As a matter of fact, a CD spectrum of unordered conformation was obtained at 80 °C (Figure S5A, gray bold line). As will be reported below, rheological measurements showed a thermal gel-sol transition in the same range of temperature. These results suggest that the increase in temperature determines the breakdown of the hydrogen bond network that stabilizes the β-sheet conformation and the contemporary breaking of the entangled structure of the gel.

FT-IR measurements. The conformational analysis was also carried out by vibrational spectroscopy in ATR mode and compared with the CD results.

To this purpose ATR FT-IR spectra on dried films of C_{12}-GG**SK** obtained by deposition of solutions at some representative pHs were recorded in the spectral region of amide I and II bands (Figure S6A) in parallel with the CD spectra of the solutions (Figure S6B). The parallel amide I band around 1650 cm^{-1} proved that at acid pHs (3.4 and 6.2) the peptide headgroup was in random coil conformation whilst the strong band shifted around 1630 cm^{-1} confirmed the transition towards β-like conformation at basic pH in agreement with the CD band evolution.

DLS measurements. DLS measurements were carried out on aqueous solutions of C_{12}-GG**SK** at a concentration of 10 $mg \cdot mL^{-1}$ ($1.6 \cdot 10^{-2}$ $mol \cdot L^{-1}$) and pH 3. The lipopeptide solutions were sonicated for 5 minutes and repeatedly filtered with 0.45 μm filters. Two populations with hydrodynamic diameter (D_h) of around 5 and 90 nm were shown by CONTIN analysis of the

autocorrelation function measured at a scattering angle of 90° (Figure 3A). To emphasize the smaller nano-particle population, the sample was further filtered with 0.1 and 0.03 μm filters. As reported in Figure 3B, only the 5-nm aggregate was observed in the filtered sample. Considering that the length of the lipopeptide in its extended form is around 3 nm, the latter population is compatible with an arrangement of the lipopeptide into spherical micelles. This result is in agreement with those previously reported on other pH-sensitive lipopeptides.[24,26] The 90-nm population could be ascribed to the coexistence in solution of much longer rod-like aggregates as confirmed by TEM and SAXS results reported further in this work.

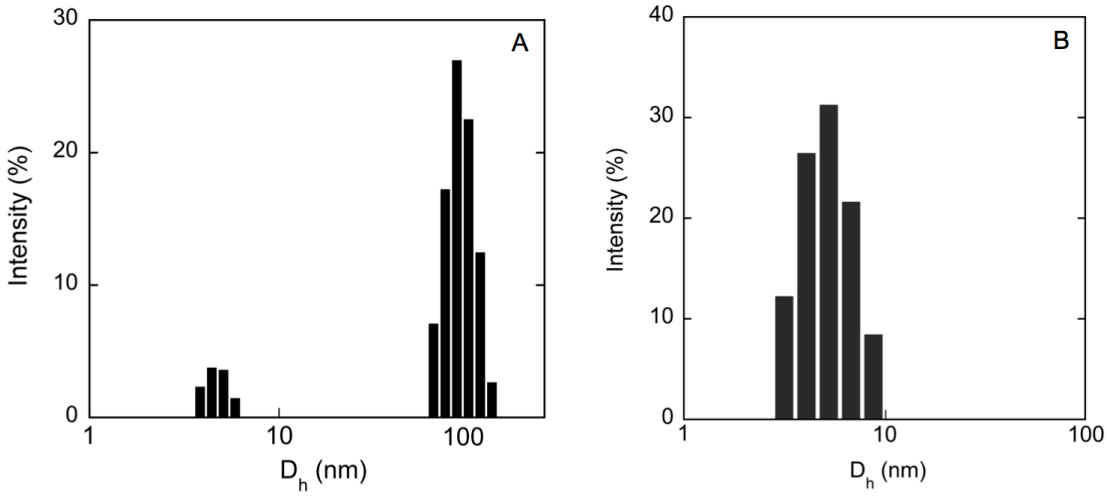

Figure 3. Distribution function of hydrodynamic diameters achieved by CONTIN analysis of DLS data for a scattering angle of 90° of an aqueous solution of C_{12}-GG**SK** at a concentration of 10 mg·mL^{-1} (1.6·10^{-2} mol·L^{-1}) and pH 3 filtered with 0.45-μm filters (A) and further filtered with 0.1- and 0.03-μm filters (B).

Evaluation of cac by fluorescence spectroscopy. The cac of C_{12}-GG**SK** TFA salt in water solution was determined by fluorescence spectroscopy by using the pyrene as a probe, the vibronic bands of which have relative intensity sensitive to the different hydrophobicity of the

environment.[43] The intensity ratio I_3/I_1, (where I_3 and I_1 are the intensities of the third and the first vibronic bands recorded at the wavelength of 384 e 373 nm, respectively), was measured in $5 \cdot 10^{-7}$ mol·L^{-1} aqueous solutions of pyrene and different concentration of the conjugate in the range $2.0 \cdot 10^{-6}$ and $4.0 \cdot 10^{-3}$ mol·L^{-1} (Figure 4).

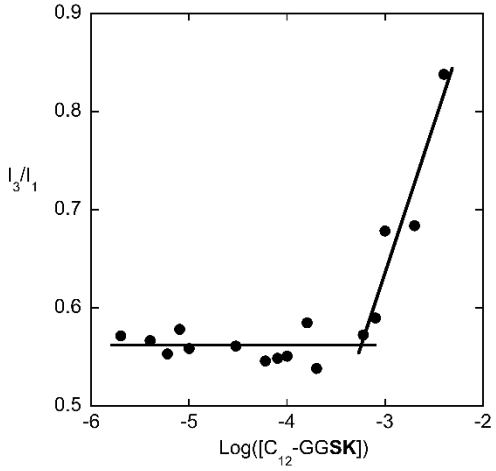

Figure 4. Trend of intensity ratio I_3/I_1 (I_{384}/I_{373}) of pyrene versus the concentration of aqueous solutions of C_{12}-GG**SK** at spontaneous pH. The break point indicates a cac value of $6.0 \cdot 10^{-4}$ mol·L^{-1}.

The cac was $6.0 \cdot 10^{-4}$ mol·L^{-1} as estimated by the break point in the concentration dependence of the intensity ratio I_3/I_1. This value is largely compatible, although slightly higher, with cac values reported for other lysine-containing palmitoyl peptides such as C_{16}-Gly-His-Lys, C_{16}-Lys-Thr and C_{16}-Lys-Thr-Lys-Ser investigated by Castelletto *et al*.[19] For lipopeptides with similar hydrophilic peptide headgroups, in fact, cac strongly depends on the length of the lipidic chain.

Morphological analysis of nano-aggregates and gel. The morphology of nano-aggregates was evaluated by TEM measurements achieved by deposition of C_{12}-GG**SK** water solutions at

two different concentrations, higher than cac, where pH was modified by addition of NaOH solutions.

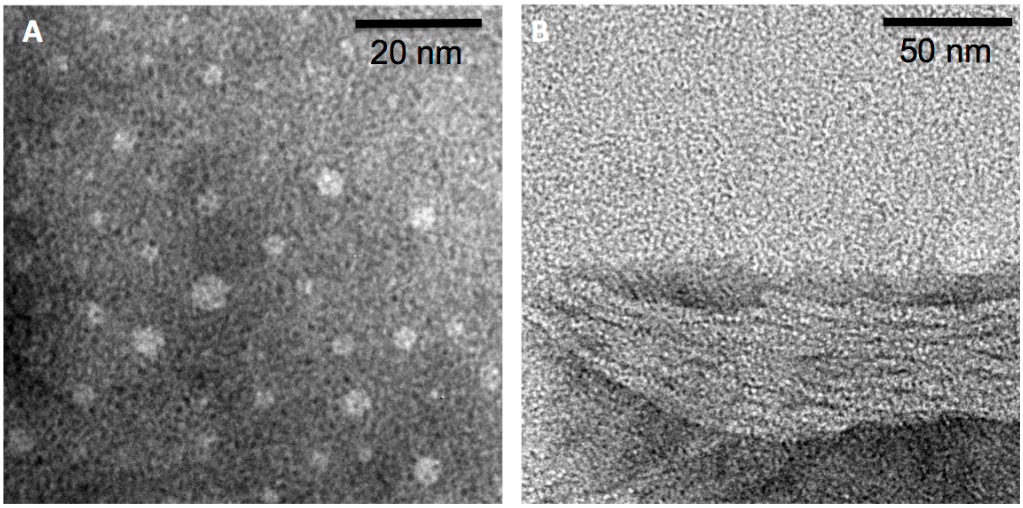

Figure 5. Negatively stained TEM micrographs achieved by deposition of C_{12}-GG**SK** water solutions at pH around 3 and concentration of $7.0 \cdot 10^{-4}$ mol·L^{-1} (A) and $1.6 \cdot 10^{-3}$ mol·L^{-1} (B). Staining was obtained with 2% w/v PTA buffered at pH 7.3.

Figure 5 and Figure S7 show some negatively stained TEM micrographs obtained by deposition of pH 3 solutions at $7.0 \cdot 10^{-4}$ mol·L^{-1} (A) and $1.6 \cdot 10^{-3}$ mol·L^{-1} (B). TEM images obtained by the former solution and more diluted ones (Figure 5A and S7A) showed that C_{12}-GG**SK** at acid pH self-organizes into spherical micelles with an average diameter of about 5 nm confirming the results provided by DLS measurements. However, despite electrostatic repulsions due to the charged lysines favor micellar aggregates at acid pH, TEM micrographs evidenced the presence of fibrous structures with about 5 nm thickness and hundreds nanometer length at higher C_{12}-GG**SK** concentration (Figures 5B and S7B) as previously suggested.[52] The appearance of the cylindrical aggregates justifies the presence of the peak at larger size (90 nm) together with that assignable to the spherical micelles in the DLS size distribution (Figure 3A). It is possible to speculate that stronger hydrophobic interactions consequent to concentration effects

could compensate weak hydrogen bond interactions. These concepts were previously demonstrated by Velichko *et al*. by Montecarlo simulations adopting a coarse-grained model to build a theoretical phase diagram that includes spherical and cylindrical micelles according to the equilibrium between hydrophobic and hydrogen bonding strength.[53]

Some TEM micrographs collected on basic solution deposition (pH 8.4) are shown in Figure 6A and B for a concentration of $7.0 \cdot 10^{-4}$ mol·L^{-1} and in Figure 6C and D for a concentration of $1.6 \cdot 10^{-3}$ mol·L^{-1}. At this pH, where the lysine residues are still partially charged, the lipopeptide C_{12}-GG**SK** self-assembles exclusively into long fibers with an average thickness of about 4.5-5 nm. In addition, TEM images revealed supercoiled fibers (Figure S8). This structural motif could be imposed by the residual charged headgroups to reduce the electrostatic repulsions when the chains overlap and by the propensity of the β-sheet strands to twist.[54]

The fibers density remarkably increases by increasing the C_{12}-GG**SK** concentration from $7.0 \cdot 10^{-4}$ to $1.6 \cdot 10^{-3}$ mol·L^{-1}, thus providing a particularly thick network of intertwined fibrils at the higher concentration (Figure 6C and D and Figure S9). Theoretical and experimental investigations in fact demonstrated the critical role of the balance between the electrostatic interactions and the hydrogen bonds in the peptide amphiphile self-assembling. Fibrils are obtained when the electrostatic repulsions between the charged headgroups are weak and hydrogen bond interaction dominates. On the contrary, the formation of spherical micelles is possible in the presence of weak hydrogen bonds and strong electrostatic repulsions.[9,13,23,39] Then, transitions from spherical micelles to fibrils can be achieved by tuning the ionic strength and pH, which controls the charge of the lipopeptide polar head as in this work.

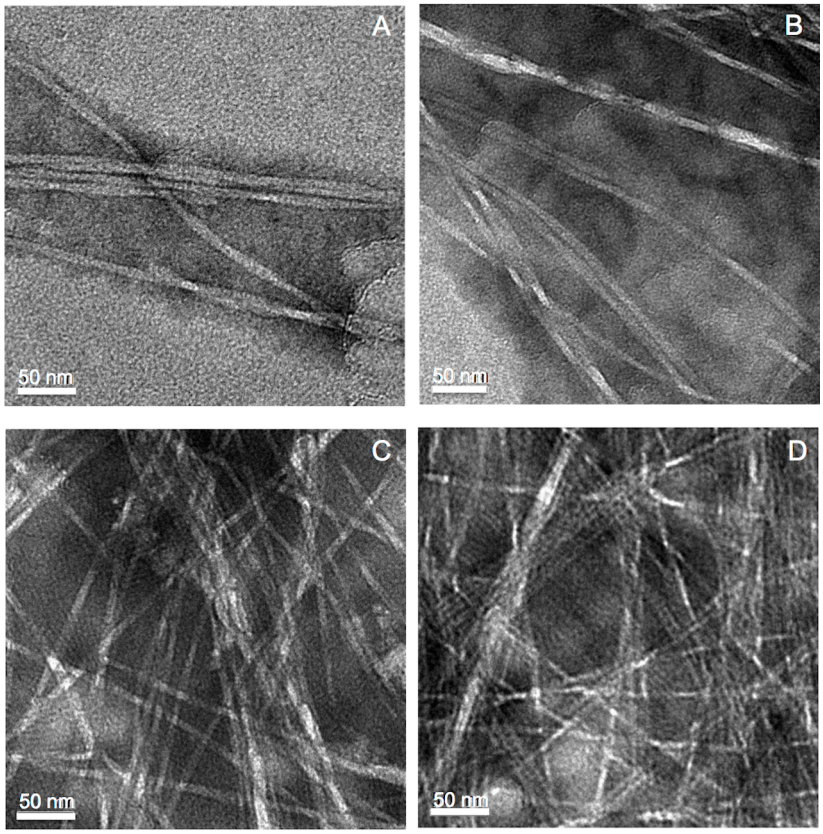

Figure 6. Examples of negatively stained TEM micrographs achieved by deposition of C_{12}-GG**SK** water solutions at pH 8.4 and concentration of $7.0 \cdot 10^{-4}$ mol·L^{-1} (A and B) and $1.6 \cdot 10^{-3}$ mol·L^{-1} (C and D). Staining was obtained with 2% w/v PTA buffered at pH 7.3.

The whole set of TEM findings was in agreement with CD and FT-IR measurements that highlighted the peptide transition from disordered to *β*-like conformation either increasing pH or lipopeptide concentration. They also explained the enhancement of viscosity or the formation of gels observed at sufficiently high pH and concentration.

SEM analysis was employed to investigate the nano-structure of the hydrogel obtained at relatively high concentration ($3.1 \cdot 10^{-3}$ mol·L^{-1}) and pH 11.0, after freezing the sample in liquid nitrogen, freeze-fracturing and freeze-drying in high vacuum (Figure S10). In agreement with TEM results, a highly intertwined network of fibers was observed in the dried gel, although with

a larger average thickness of 15-20 nm. In fact, the absence of electrostatic repulsions due to the uncharged lysines at basic pH favor lateral adhesion.

SAXS measurements. SAXS data were collected on solution at acid and basic pH after sol-gel transition, to provide complementary analysis of the aggregate structures.

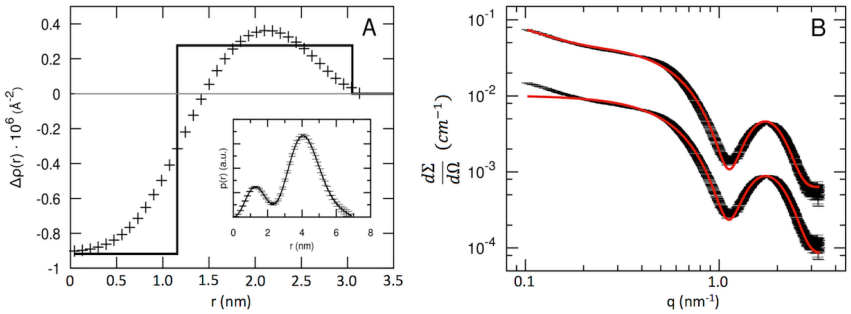

Figure 7. (A) Pair distribution function for C_{12}-GG**SK** at acidic pH (insert); radial electronic density contrast obtained from the model fitting (line) and extracted from the $p(r)$ function (insert) by using the program DECON (crosses).[55] The zero level is defined by the scattering-length density of the solvent ($\rho_{water} = 9.43 \cdot 10^{-6}$ Å^{-2}). (B) Experimental and calculated scattering intensities for a core-shell spherical model (bottom) and with a cylindrical particle contribute (top). The pattern on top is shifted along the ordinate axis. The water solution was 25 mg·mL^{-1} at spontaneous pH. The intensity in absolute units is normalized for this value. The pattern on top is shifted along the ordinate axis.

The ITP analysis of the scattered intensity curve for solutions of C_{12}-GG**SK** at acidic pH provided a $p(r)$ function that was consistent with globular particles with a core-shell structure (Figure 7A, inset), a maximum dimension of 6.5 nm and a derived gyration radius of 2.80±0.05 nm. The radial electron density contrast profile Δρ(r) was extracted from the $p(r)$ curves (inset of Figure 7A), by using the program DECON[55] based on the so-called Convolution Square Root

method[56-57] and widely employed to deconvolute pair distance distribution functions of inhomogeneous scattering particles.[58,59]

The obtained Δρ(r) (Figure 7A) shows a typical core-shell profile, where the electron density of the core and the shell are lower and higher than that of the solvent, respectively. The scattered intensity could be also reproduced by assuming a form factor of core-shell spherical particles with a core radius of 1.16±0.05 nm and a shell thickness of 1.90±0.06 nm (Figure 7B). Gaussian polydispersity parameters (0.1±0.01 were included in the fit for both core radius and shell thickness (Figure 7B, bottom). The best fitting radial electron density contrast is in agreement with the profile obtained by the deconvolution of the $p(r)$ function (Figure 7A). Both the maximum distance and the total radius obtained with the model based fit (6.12±0.05 nm) are in reasonable agreement with the size inferred from the micelle TEM images (Figure 5A) and DLS results (peak at 5 nm of Figure 3) collected on the C_{12}-GG**SK** samples at low pH.

The model fitting can be improved at low q values (Figure 7B, top) by adding a contribution (6%) of a practically infinitely long cylinder, representing the elongated structures detected in small fraction by TEM (Figure 5B) and DLS (peak at larger size of Figure 3A) in similar sample conditions. A cylinder cross-section with a core-shell structure similar to that of the spherical aggregate and a slightly larger thickness (2.5 ± 0.06 nm) provided the best fit.

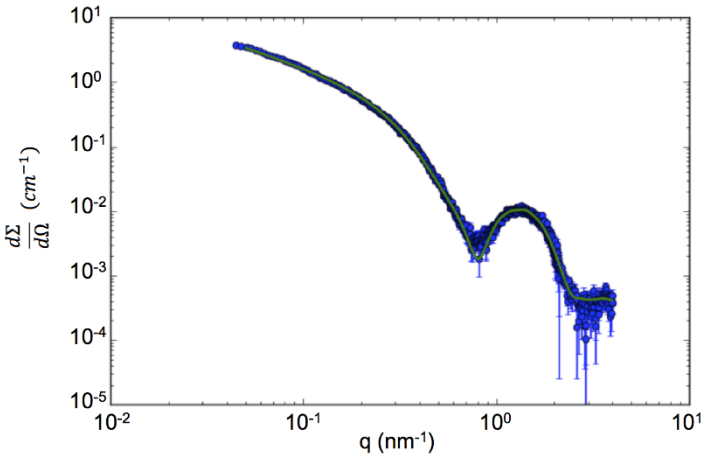

Figure 8. Experimental scattering intensities (black dots with error bars) for C_{12}-GG**SK** at pH 11 and 3.8 mg·mL^{-1} and calculated profile (blue line) for a core-shell ribbon model. The intensity in absolute units is normalized for the concentration value.

The transition from solution to gel, obtained by increasing the pH to 11, led to a different SAXS profile (Figure 8), which suggested the presence of elongated structures, in agreement with the TEM results. The scattered intensity could be well reproduced (Figure 8) by assuming a form factor of infinitely long fibers with a rectangular cross-section and a core shell structure along the thickness. The model provided an agreement factor χ^2=1.29 when it was used to fit the experimental curve in the q-range 0.05<q<4 nm^{-1}. The cross-section as a whole was 7.40 ± 0.06 nm thick and 14.80 ± 0.06 nm wide. The core-shell distribution of the electron density along the thickness foresees a central region of 5.75 ± 0.03 nm and two shells at the two extremities of 0.84 ± 0.04 nm.

We anticipate that this distribution mimics a complex one of the electron density provided by a head-tail-tail-head packing of the molecules in the rod-like aggregates. With a scattering-length density of the solvent ϱ_{water} = 9.43·10^{-6} Å^{-2}, the obtained $\Delta\varrho(r)$ (1.6·10^{-6} Å^{-2} and -0.6·10^{-6} Å^{-2}) for the head and tail regions show an electron density of the heads and the tail which are higher and

lower than that of the solvent, respectively. The ratio of the $\Delta\varrho(r)$ (2.6) is not excessively far from the ratio found for the core-shell micelles.

Attempts to fit the collected data with a cylindrical core-shell cross-section or a lamellar structure did not give good agreements. The plausibility of a certain structural model can be assessed by a simple check with the Guinier plots for elongated objects with two finite dimensions (cylinders, long prisms) and for lamellar cross-sections. In this case the linear fits provided gyration radii R_c and R_t of 4.75 and 2.47 nm, respectively. Even if the cross-section is not homogeneous, a rough comparison could be decisive. The R_c of a homogeneous infinitely long parallelepiped with calculated dimensions of the cross section 7.4×14.8 nm would be 4.78 nm (in agreement with the experimental value), whereas a measured R_t of 2.47 nm would correspond to a homogeneous thickness of 8.5 nm.

Rheological analysis on lipopeptide hydrogels. Rheological properties of the lipopeptide C_{12}-GG**SK** were investigated at basic pH since the sol-gel transitions occur at high pH only. The stability of the gel as a function of temperature was investigated to compare rheological and CD spectroscopy results. In fact, it seems apparent that the gel forms when the conformational transition from random coil to β-sheet structures occurs, as will be clarified below. Rheological measurements were carried out on $3.2 \cdot 10^{-3}$ mol·L^{-1} (2 mg·mL^{-1}) C_{12}-GG**SK**. The solution was brought at pH 11 with concentrated NaOH solution and left overnight before the measurement. A frequency sweep experiment allowed the measurement of the elastic (G') and viscous modulus (G'') and their dependence on the frequency in the range 0.1-10 Hz (Figure 9A). Both moduli were almost independent of the frequency and the elastic modulus was of an order of magnitude larger than the viscous modulus; this result demonstrates that the gel is strong.[41] The value of the elastic modulus around 100 Pa indicates the formation of a rather flexible gel.

A temperature scan from 25 to 78 °C was run on this gel at the frequency of 1 Hz obtaining the trend reported in Figure 9B. The steep decreasing of G' of about 5 order of magnitude at around 50 °C revealed a cooperative transition consequent to the melting of the gel. The melting temperature is in good agreement with that obtained by the thermal denaturation measured on the C_{12}-GG**SK** gel by CD spectroscopy (Figure S5B) suggesting that the conformational transition towards β-like structures of the peptide headgroup promotes the gel formation.

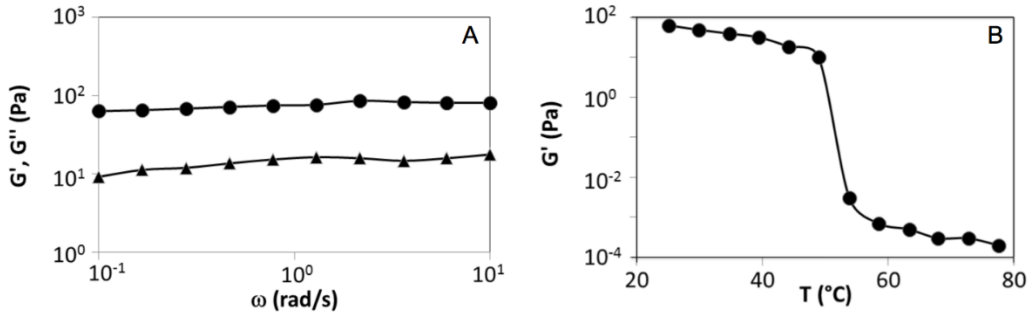

Figure 9. (A) G' (—●—) and G'' (—▲—) measured with a frequency sweep experiment carried out on $3.2 \cdot 10^{-3}$ mol·L^{-1} (2 mg·mL^{-1}) C_{12}-GG**SK** solution filtered with a 0.45 μm filter. T=25 °C. (B) Trend of G' as a function of temperature. Temperature scan speed=0.1 °C·min^{-1}, frequency =1 Hz, γ=0.001.

The thermal effects produced a gel-sol transition following the weakening of the hydrogen bond interactions and a consequent loss of the peptide moiety ordered structure. This behavior seems to substantiate that C_{12}-GG**SK** could self-organize into core-shell aggregates that undergo remodeling from spherical micelles to fibrous structures to gel consisting of a complex entanglement of fibers in response to pH and concentration as previously reported for other lipopeptides[39,60-65] and lipid-based conjugates.[66]

MD simulations. All-atom MD simulations were performed for C_{12}-GG**SK** in water to investigate in more details the structure of rod-like aggregates as evidenced by TEM micrographs at basic pH.

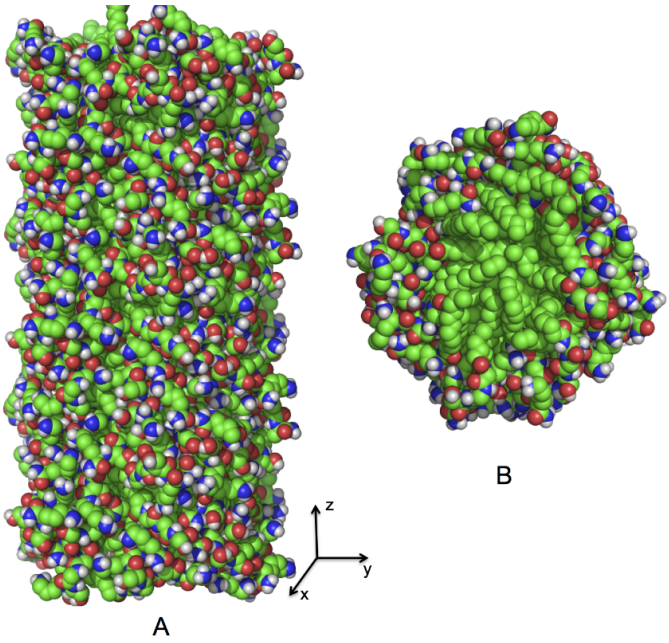

Figure 10. Rod-like structure of assembled C_{12}-GG**SK** in water as obtained after 50 ns MD simulations in lateral (A) and top (B) view. The alkyl core is rendered in green. The molecular structure was provided using the PyMol Molecular Graphics System.[51]

72 parallel lipopeptide molecules were preassembled in cylindrical structure and adopted as the initial condition for the MD simulations (Figure S4). This structure was considered as the representative section of an infinitely long rod with core-shell morphology. To this end, the size of *z*-axis (perpendicular to the top surface of the rod) was adjusted to have van der Waals distances between each adjacent cell whilst the *x*- and *y*-axis were large enough to avoid lateral adhesion of the aggregates.

The 50 ns MD simulation in water provided a lipopeptide aggregate with a slightly distorted cylindrical structure with a core-shell morphology (Figure 10). The structural features of the assembled lipopeptides were analyzed and compared with those of the initial condition. A sharp increase of the number of hydrogen bonds occurs in the first 15 ns MD simulation reaching the maximum number of ≈4 hydrogen bonds per lipopeptide molecule. As a consequence, the symmetry of the initial structure broke and a long fiber was obtained. The structure is in fact characterized by a value of the ratio of the principal moments of inertia, $I_x/I_{y,}$ around 0.9, which suggests an almost cylindrical shape of the aggregate. The hydrophobic core has a diameter of about 3.4 nm, which indicates a partial interdigitation of the lipidic chains, if compared with the value of 4.4 nm, coherent with completely elongated chains, of the starting structure. The cylindrical structure has a diameter of 5.5 nm, strongly reduced with respect to the initial value of 7.4 nm. These findings are consistent with TEM results obtained by deposition of C_{12}-GG**SK** water solutions at pH 8.4 that provided a lower thickness of 4.5-5.0 nm, probably due to shrinking effects.

CONCLUSIONS

Herein the self-assembling behavior in water of the new lipopeptide C_{12}-GG**SK** was described. C_{12}-GG**SK** self-organizes into polymorphic aggregates in response to changes of pH, concentration and temperature. The pH-dependent transition from random coil to β-sheet conformation of the peptide moiety, shown by circular dichroism and vibrational spectroscopy, induced morphological remodeling of the self-aggregates in water. The morphology of the self-assemblies was also sensitive to the concentration of the lipopeptide.

Possible structural models of the self-assemblies are illustrated in Figure 11. Spherical micelles and a smaller fraction of cylindrical micelles, obtained at higher concentration, were revealed at acid pH by DLS, TEM and SAXS measurements.

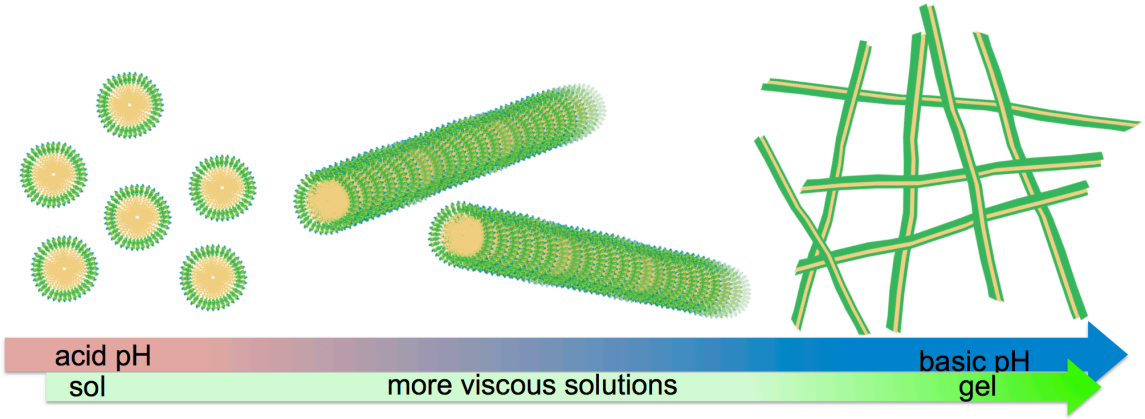

Figure 11. Schematic structures of self-aggregates formed by self-assembling C_{12}-GG**SK** in water when pH was increased. From left to right spherical micelles at acid pH, a rod-like structure at pH≈8, as shown by TEM results, entangled ribbons, as inferred by SAXS, for the gel fibers obtained at pH 11.

The increase of pH and concentration gave rise to more viscous solutions suggesting the formation of a network of aligned and intertwined fibers, as revealed by TEM micrographs collected at pH 8.4, when the lysine residues are still partially charged. In these conditions, C_{12}-GG**SK** self-assembles exclusively into long fibers with an average thickness of about 4.5-5 nm, compatible with structural details obtained by MD simulations performed on the uncharged lipopeptide in water. At pH 10-11 and rather high concentration, a medium strength gel with head-tail-tail-head structure, as inferred by SAXS, was obtained.

The versatility of C_{12}-GG**SK**, which self-organizes into assemblies whose size and shape can be modified in response to pH, concentration and temperature, and the high stability of the self-

assemblies due to the lipidation make this lipopeptide a promising candidate to use in therapeutics as drug carrier and gene vector, due to the presence of positively charged lysines. Furthermore, the ε-amino group of the lysine residue allows cross-linking of self-aggregates at different extent providing gels with increased strength with possible applications in tissue engineering.

AUTHOR INFORMATION

Corresponding Author

* E-mail: giancarlo.masci@uniroma1.it

* E-mail: anita.scipioni@uniroma1.it

Present Address

[¥] Centro Singular de Investigatiòn en Quimica Biolòxica e Materiais Moleculares, Santiago de Compostela, Spain

[◇] Department of Chemistry, Maynooth University, Maynooth, Co. Kildare, Ireland

[§] Dipartimento di Ingegneria, Università di Roma Tre, Via V. Volterra, 62, Rome, Italy

ACKNOWLEDGMENTS

The authors acknowledge Prof. R. Caminiti (Chemistry Dept., Sapienza University of Rome) for providing free computing time on NARTEN Cluster HPC Facility and Dr. Francesco Mura (CNIS Laboratory of Sapienza University of Rome). This work was supported by Fondi Ateneo Sapienza 2016 and 2017. Parts of this research were carried out at the SWING beamline at SOLEIL. We would like to thank J. Perez for assistance during the experiment. This work

benefited from the use of the SasView application, originally developed under NSF award DMR-0520547. SasView contains code developed with funding from the European Union's Horizon 2020 research and innovation programme under the SINE2020 project, grant agreement No 654000.

REFERENCES

(1) Rad-Malekshahi, M.; Lempsink, L.; Amidi, M.; Hennink, W.E.; Mastrobattista, E. Biomedical Applications of Self-Assembling Peptides. *Bioconjug. Chem.* **2016**, *27*, 3-18.

(2) Sun, L.; Zheng, C.; Webster, T.J. Self-Assembled Peptide Nanomaterials for Biomedical Applications: Promises and Pitfalls. *Int. J. Nanomedicine* **2017**, *12*, 73-86.

(3) Edwards-Gayle, C.J.C.; Hamley, I.W. Self-Assembly of Bioactive Peptides, Peptide Conjugates, and Peptide Mimetic Materials. *Org. Biomol. Chem.* **2017**, *15*, 5867-5876.

(4) Nyström, L.; Malmsten, M. Membrane Interactions and Cell Selectivity of Amphiphilic Anticancer Peptides. *Curr. Opin. Colloid Interface Sci.* **2018**, *38*, 1-17.

(5) Qiu, F.; Chen, Y.; Tang, C.; Zhao, X. Amphiphilic Peptides as Novel Nanomaterials, Design, Self-assembly and Application. *Int. J. Nanomed.* **2018**, *13*, 5003-5022.

(6) Mathur, D.; Prakash, S.; Anand, P.; Kaur, H.; Agrawal, P.; Mehta, A.; Kumar, R.; Singh, S.; Raghava, G.P.S. PEPlife: A Repository of the Half-life of Peptides. *Scientific Reports*, **2016**, *6:36617*, 1-7.

(7) Jing, X.; Foged, C.; Martin-Bertelsen, B.; Yaghmur, A.; Knapp, K.M.; Malmsten, M.; Franzyk, H.; Nielsen, H.M. Delivery of siRNA Complexed with Palmitoylated α-Peptide/β-Peptoid Cell-Penetrating Peptidomimetics: Membrane Interaction and Structural Characterization of a Lipid-Based Nanocarrier System. *Mol. Pharmaceutics* **2016**, *13*, 739-1749.

(8) Hendricks, M.P.; Sato, K.; Palmer, L.C.; Stupp, S.I. Supramolecular Assembly of Peptide Amphiphiles. *Acc. Chem. Res.* **2017**, *50*, 2440-2448.

(9) Armas, F.; Pacor, S.; Ferrari, E.; Guida, F.; Perthinez, T.A.; Romani, A.A.; Scocchi, M.; Benincasa, M. Design, Antimicrobial and Mechanism of Action of Arg-rich Ultra-Short Cationic Lipopeptides. *PLos ONE* **2019**, *14*, e0212447.

(10) Sato, K.; Hendricks, M.P.; Palmer, L.C.; Stupp, S.I. Peptide Supramolecular Materials for Therapeutics. *Chem Soc. Rev.* **2018**, *47*, 7539-75551.

(11) Hartgerink, J.D.; Beniash, E.; Stupp, S.I. Self-assembly and Mineralization of Peptide-Amphiphile Nanofibers. *Science* **2001**, *294*, 1684-1688.

(12) Dasgupta, A.; Debratim, D. Designer Peptide Amphiphile: Self-assembly to Applications. *Langmuir* **2019**, *35*, 10704-10724.

(13) Cui, H.; Webber, M.J.; Stupp, S.I. Self-assembly of Peptide Amphiphiles: from Molecules to Nanostructures to Biomaterials. *Biopolymers (Pept Sci)* **2010**, *94*, 1-18.

(14) Perez, C.M.R.; Alvarez, Z.; Chen, F.; Aytun, T.; Stupp, S.I. Mimicking the Bioactivity of Fibroplast Growth Factor-2 Using Supramolecular Nanoribbons. *ACS Biomat. Sci. Eng.* **2017**, *3*, 2166-2175.

(15) Acar, H.; Srivastava, S.; Chung, E.J.; Schnoremberg, M.R.; Barret, J.C.; LaBelle, J.L.; Tirrell, M. Self-Assembling Peptide-Based Building Blocks in Medical Applications. *Adv. Drug. Deliv. Rev.* **2017**, *110-111*, 65-79.

(16) Varvaresou, A.; Iakovou, K. Biosurfactants in Cosmetics And Biopharmaceuticals. *Letters in Applied Microbiology* **2015**, *61,* 214-223.

(17) Kanlayavattanakul, M.; Lourith, N. Lipopeptides in Cosmetics. *Int. J. Cosmet. Sci.* **2009**, *31*, 255-261.

(18) Palladino, P.; Castelletto, V.; Dehsorkhi, A.; Stetsenko, D.; Hamley, I. W. Conformation and Self-Association of Peptide Amphiphiles Based on the KTTKS Collagen Sequence. *Langmuir* **2012**, *28*, 12209-12215.

(19) Castelletto, V.; Hamley, I.W.; Whitehouse, C.; Matts, P.J.; Osborne, R.; Baker, E.S.; Self-Assembly of Palmitoyl Lipopeptides Used in Skin Care Products. *Langmuir* **2013**, *29*, 9149-9155.

(20) Hamley, I.W.; Dehsorkhi, A.; Castelletto, V.; Walter, M.N.M.; Connon, C.J.; Reza, M.; Ruokolainen, J. Self-Assembly and Collagen-Stimulating Activity of a Peptide Amphiphile Incorporating a Peptide Sequence from Lumican. *Langmuir* **2015**, *31*, 4490-4495.

(21) Avrahami, D.; Shai, Y. A New Group of Antifungal and Antibacterial Lipopeptides Derived from Non-Membrane Active Peptide Conjugated with Palmitic Acid. *J. Biol. Chem.* **2004**, *279*, 12277-12285.

(22) Hamley, I.W. Lipopeptides: from Self-Assembly to Bioactivity. *Chem. Commun.* **2015**, *51*, 8574–8583.

(23) Hartgerink, J.D.; Beniash, E.; Stupp, S.I. Peptide-Amphiphile Nanofibers: a Versatile Scaffold for the Preparation of Self-Assembling Materials. *Proc. Natl. Acad. Sci. USA* **2002**, *99*, 5133-5138.

(24) Tsonchev, S.; Niece, K.L.; Schatz, G.C.; Ratner, M.A.; Stupp, S.I. Phase Diagram for Assembly of Biologically-Active Peptide Amphiphiles. *J. Phys. Chem. B* **2008**, *112*, 441-447.

(25) Dehsorkhi, A.; Castelletto, V.; Hamley I.W. Self-Assembling Amphiphilic Peptides. *J. Pept. Sci.* **2014**, 20, 453-467.

(26) Ghosh, A.; Haverick, M.; Stump, K.; Yang, X.; Tweedle, M. F.; Goldberger J. E. Fine-Tuning the pH Trigger of Self-Assembly. *J. Am. Chem. Soc.* **2012**, *134*, 3647-3650.

(27) Jin, Hue; Xu, X-D; Chen, C-S; Cheng, S-X; Zhang, X-Z; Zhou, R-X. Bioactive Peptide Derivatives with pH Triggered Morphology and Structure. *Macromol. Rapid Commun.* **2008**, *29*, 1726-1731.

(28) Qin, S-Y; Xu, S-S; Zhuo, R-X; Zhang, X-Z. Morphology Transformation Via pH-Triggered Self-Assembly of Peptides. *Langmuir* **2012**, *28*, 2083-2090.

(29) Gosh, A.; Buettner, C. J.; Manos, A. A.; Wallace, A. J.; Tweedle, M. F.; Goldberger, J. E. Probing Peptide Amphiphile Self-Assembly in Blood Serum. *Biomacromolecules* **2014**, *15*, 4488-4494.

(30) Moyer, T. J.; Finbloom, J. A.; Chen, F.; Toft, D. J.; Cryns, V. L.; Stupp, S. I. pH and Amphiphilic Structure Direct Supramolecular Behavior in Biofunctional Assemblies. *J. Am. Chem. Soc.* **2014**, *136*, 14746-14752.

(31) Gosh, A.; Dobson, E. T.; Buettner, C. J.; Nicholl, M. J.; Goldberger, J. E. Programming pH-Triggered Self-Assembly Transitions Via Isomerization of Peptide Sequence. *Langmuir* **2014**, *30*, 15383-15387.

(32) Forns, P.; Lauer-Fields, J.L.; Gao, S.; Fields, G.B. Induction of Protein-Like Molecular Architecture by Monoalkyl Hydrocarbon Chains. *Biopolymers* **2000**, *54*, 531-546.

(33) Xu, X.; Jin, Y.; Liu, Y.; Zhang, X.; Zhuo, R. Self-Assembly Behavior of Peptide Amphiphiles (PAs) with Different Length of Hydrophobic Alkyl Tails. *Colloids and Surfaces B: Biointerfaces* **2010**, *81*, 329-335.

(34) Castelletto, V.; Kaur, Kowalczyk, A.; R.M.; Hamley, I.W.; Reza, M.; Ruokolainen, J. Supramolecular Hydrogel Formation in a Series of Self-Assembling Lipopeptides with Varying Lipid Chain Length. *Biomacromolecules* **2017**, *18*, 2013-2023.

(35) Travaglini, L.; D'Annibale, A.; di Gregorio, M.C.; Schillén, K.; Olsson, U.; Sennato, S.; Pavel, N.V.; Galantini, L. Between Peptides and Bile Acids: Self-Assembly of Phenylalanine Substituted Cholic Acids. *J. Phys. Chem. B* **2013**, *117*, 9248-9257.

(36) Travaglini, L.; Giordano, C.; D'Annibale, A.; Gubitosi, M.; di Gregorio, M.C.; Schillén, K.; Stefanucci, A.; Mollica, A.; Pavel, N.V.; Galantini, L. Twisted Nanoribbons from a RGD-Bearing Cholic Acid Derivative. *Colloids and Surfaces B: Biointerfaces* **2017**, *159*, 183-190.

(37) Shimada, T.; Lee, S.; Bates, F.S.; Hotta, A.; Tirrel, M. Wormlike Micelle Formation in Peptide-Lipid Conjugates Driven by Secondary Structure Transformation of the Headgroups. *J. Phys. Chem. B* **2009**, *113*, 13711-13714.

(38) Missirlis, D.; Chworos, A.; Fu, C.J.; Khant, H.A.; Krogstad, D.V.; Tirrell, M. Effect of the Peptide Secondary Structure on the Peptide Amphiphile Supramolecular Structure and Interactions. *Langmuir* **2011**, *27*, 6163-6170.

(39) Paramonov, S.; Jun, H.; Hartgerink, J.D. Self-Assembly of Peptide-Amphiphile Nanofibers: The Roles of Hydrogen Bonding and Amphiphilic Packing. J. *Am. Chem. Soc. 128*, **2006**, 7291-7298.

(40) Qi, R.; Liu, J.; Zhang, N.; Ji, X.; Han, Y.; Wang, Y. Assembly and Evolution of Gemini-Type Peptide Amphiphile with a di-Lysine Spacer. *Langmuir* **2019**, *35*, 6154-6160.

(41) Raghavan, S.R.; Douglas, J.F. The Conundrum of Gel Formation by Molecular Nanofibers, Wormlike Micelles, and Filamentous Proteins: Gelation without Cross-Links? *Soft Matter* **2012**, *8*, 8539-8546.

(42) Aulisa, L.; Dong, H.; Hartgerink, J. D. Self-Assembly of Multidomain Peptides: Sequence Variation Allows Control over Cross-Linking and Viscoelasticity. *Biomacromolecules* **2009**, *10*, 19447-19454.

(43) Kalyanasundaram, K.; Thomas, J.K. Environmental Effects on Vibronic Band Intensities in Pyrene Monomer Fluorescence and Their Application in Studies of Micellar Systems. *J. Am. Chem. Soc.* **1977**, *99,* 2039-2044.

(44) Glatter, O. A New Method for the Evaluation of Small-Angle Scattering Data. *J. Appl. Crystallogr.* **1977**, *10*, 415-421.

(45) Pedersen, J.S. Analysis of Small-Angle Scattering Data from Colloids and Polymer Solutions: Modeling and Least-Squares Fitting. *Adv. Colloid Interface Sci.* **1997**, *70*, 171-210.

(46) Konarev, P.V.; Volkov, V.V.; Sokolova, A.V.; Koch, M.H.J.; Svergun, D.I. PRIMUS: A Windows PC-Based System for Small-Angle Scattering Data Analysis. J. *Appl. Crystallogr.* **2003**, *36*, 1277-1282.

(47) Schmidt, N.; Eichenberger, A.P.; Choutko, A.; Riniker, S.; Winger, M.; van Gunsteren, W.F. Definition and Testing of the GROMOS Force-Field Version 54A7 and 54B7. *Eur. Biophys. J.* **2011**, *40*, 843-856.

(48) Poger, D.; van Gusteren, W.F.; Mark, A.E. A New Force Field for Simulating Phosphatidylcholine Bilayers. *J. Comp. Chem.* **2010**, *31*, 1117-1125.

(49) Poger, D.; Mark, A. E. On the Validation of Molecular Dynamics Simulations of Saturated and Cis-Monoinsaturated Phosphatidylchline Lipid Bilayers: A Comparison With Experiments. *J. Chem. Theory Comput.* **2010**, *6*, 325-336.

(50) Darden, T.; York, D.; Pedersen, L. Particle Mesh Ewald: an Nlog(N) Method for Ewald Sums in Large Systems. *J. Chem. Phys.* **1993**, *98*, 10089-10092.

(51) DeLano, W. L. The PyMOL Molecular Graphics System; DeLano Scientific: San Carlos, CA, 2008. www.pymol.org

(52) Shimada, T.; Sakamoto, N.; Motokawa, R.; Koizumi, S.; Tirrell, M. Self-Assembly Process of Peptide Amphiphile Worm-Like Micelles. *J. Phys. Chem. B* **2012**, *116*, 240-244.

(53) Velichko, Y.S.; Stupp, S.I.; Olvera de la Cruz, M. Molecular Simulation Study of Peptide Amphiphile Self-assembly. *J. Phys. Chem. B* **2008**, *112*, 2326-2334.

(54) Shamovsky, I.L.; Ross, G.M.; Riopelle, R.J. Theoretical Studies on the Origin of β-Sheet Twisting. *J. Phys. Org. Chem.* **2000**, *104*, 11296-11307.

(55) Mittelbach, R.; Glatter, O. Direct Structure Analysis of Small-Angle Scattering Data from Polydisperse Colloidal Particles. *J. Appl. Crystallogr.* **1998**, *31*, 600-608.

(56) O. Glatter, Convolution Square Root of Band-Limited Symmetrical Functions and its Application to Small-Angle Scattering Data, *J. Appl. Crystallogr.* **1981**, *14*, 101-108.

(57) Glatter, O. Comparison of Two Different Methods for Direct Structure Analysis from Small-Angle Scattering Data. *J. Appl. Crystallogr.* **1988**, *21*, 886-890.

(58) Tomšič, M.; Bešter-Rogač, M.; Jamnik, A.; Kunz, W.; Touraud, D.; Bergmann, A.; Glatter, O. Ternary Systems of Nonionic Surfactant Brij 35, Water and Various Simple Alcohols: Structural Investigations by Small-Angle X-Ray Scattering and Dynamic Light Scattering. *J. Colloid Interface Sci.* **2006**, *294*, 194-211.

(59) Tomšič, M.; Bešter-Rogač, M.; Jamnik, A.; Kunz, W.; Touraud, D.; Bergmann, A.; Glatter, O. Nonionic Surfactant Brij 35 in Water and in Various Simple Alcohols: Structural Investigations by Small-Angle X-ray Scattering and Dynamic Light Scattering. *J. Phys. Chem. B.* **2004**, *108*, 7021-7032.

(60) Stendahl, J. C.; Rao, M. S.; Guler, M. O.; Stupp, S. I. Intermolecular Forces in the Self-Assembly of Peptide Amphiphile Nanofibers. *Adv. Func. Mater.* **2006**, *16*, 499-508.

(61) Behanna, H.A.; Donners, J.J.J.M.; Gordon, A.C.; Stupp, S.I. Coassembly of Amphiphiles with Opposite Peptide Polarities into Nanofibers. *J. Am. Chem. Soc. 127*, **2005**, 1193-1200.

(62) Ekiz, M.S.; Cinar, G.; Khalily, M.A.; Guler M.O. Self-Assembled Peptide Nanostructures for Functional Materials. *Nanotechnology* **2016**, *27*, 402002.

(63) Miravet, J.F.; Escuder, B.; Segarra-Maset, M. D.; Tena-Solsona, M.; Hamley, I.W.; Dehsorkhi, A.; Castelletto, V. Self-Assembly of a Peptide Amphiphile: Transition from Nanotape Fibrils to Micelles. *Soft Matter* **2013**, *9*, 3558 -3564.

(64) Gao, C.; Kewalramani, H. Li, S.; Palmer, L.C.; Dravid, V.P.; S.I.; Stupp, Olivera de la Cruz, M.; Bedzyk, M.J. Electrostatic Control of Polymorphism in Charged Amphiphile Assemblies. *J. Phys. Chem. B 121*, **2017**, 1623-1628.

(65) Hutchinson, J.A.; Burholt, S.; Hamley, I.A.; Lundback, A-K.; Uddin, S.; Gomes dos Santos, A.; Reza, M.; Setsonen, J.; Ruokolainen, J. The Effect of Lipidation on the Self-Assembly of the Gut-Derived Peptide Hormone PYY_{3-36}. *Bioconjugate Chem.* **2018**, *29*, 2296-2308.

(66) Cautela, J.; Giustini, M.; Pavel, N.V.; Palazzo, G.; Galantini, L. Wormlike Reverse Micelles in Lecithin/Bile Salt/Water Mixtures in Oil. *Colloids and Surfaces A* **2017**, *532*, 411-419.

TOC

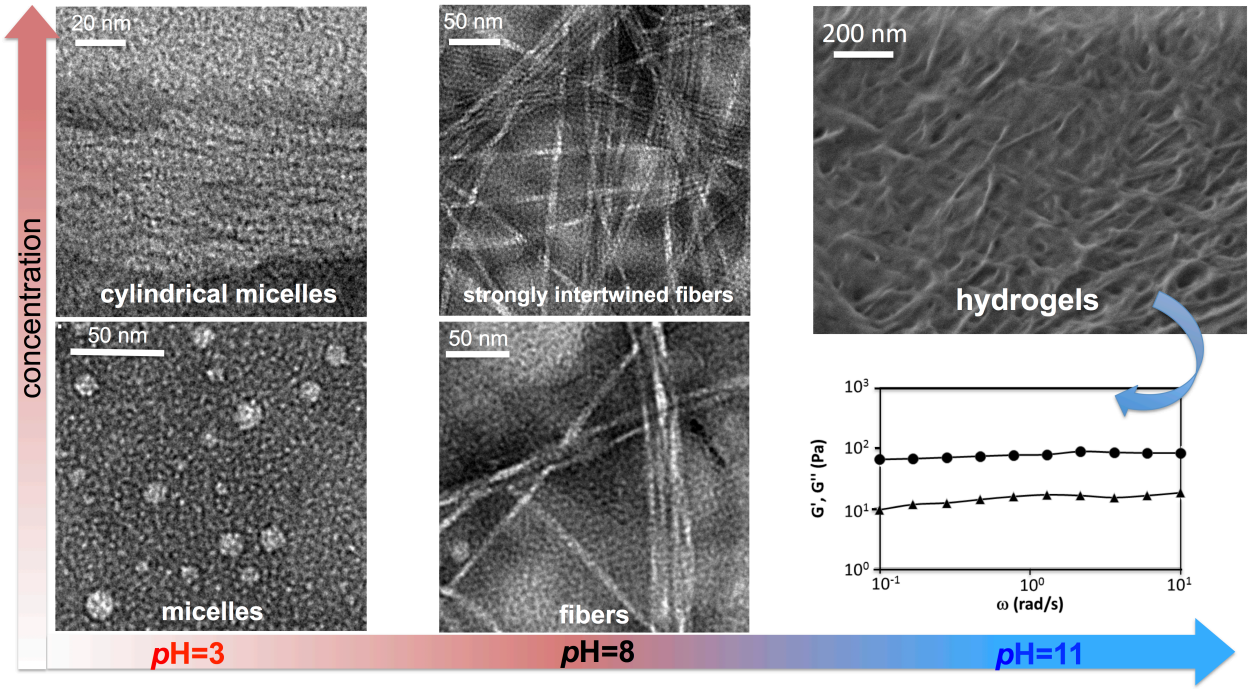
concentration
20 nm
cylindrical micelles
50 nm
micelles
50 nm
strongly intertwined fibers
50 nm
fibers
200 nm
hydrogels
G', G'' (Pa)
ω (rad/s)
pH=3
pH=8
pH=11